Formation and characterisation of Ni, Pt, and Ti stanogermanide contacts on $Ge_{0.92}Sn_{0.08}$

Emmanuele Galluccio[1], Nikolay Petkov[2], Gioele Mirabelli[1], Jessica Doherty[3], Shih-Ya Lin[4], Fang-Liang Lu[4], C.W. Liu[4], Justin D. Holmes[3,5], Ray Duffy[1]

[1] Tyndall National Institute, University College Cork, Lee Maltings, Cork, Ireland.

[2] Cork Institute of Technology, Bishopstown, Cork, Ireland.

[3] School of Chemistry, University College Cork, Cork, Ireland.

[4] Graduate Institute of Electronics Engineering, National Taiwan University, Taipei 106, Taiwan.

[5] AMBER@CRANN, Trinity College Dublin, Dublin 2, Ireland.

ABSTRACT:

In this article we provide a comparative and systematic study on contact formation for germanium-tin (GeSn) thin films containing a high percentage of Sn (8 at.%). 10 nm of Nickel (Ni), Titanium (Ti), or Platinum (Pt) was deposited on $Ge_{0.92}Sn_{0.08}$ layers grown on Ge substrates, and subsequently annealed between 300 – 500 °C to form stanogermanide alloys. Several experimental techniques were employed to characterise the material and the electrical contact behaviour, with the purpose of identifying the most promising stanogermanide contact candidate, in terms of low sheet resistance, low surface roughness and low formation temperature. Among these three different metals we found that, for nanoelectronic applications, nickel-stanogermanide (NiGeSn) was the most promising candidate based on a low sheet resistance combined with a low formation temperature, below 400 °C. PtGeSn showed better behaviour in terms of thermal stability compared with the other two options, while Ti was found to be relatively unreactive under these annealing conditions, resulting in poor TiGeSn formation. For the lowest resistance stanogermanide contact generated, namely NiGeSn formed at 300 °C, detailed lattice resolution Transmission Electron Microscopy imaging, combined with fast Fourier transformation analysis, identified the formation of the $Ni_{x-1}(GeSn)_{y-1}$ phase.

Keywords- *GeSn, stanogermanides sheet resistance, lattice imaging.*

I. INTRODUCTION

In recent years many technological breakthroughs have enabled transistor dimension scaling according to Moore's law. These innovations, such as the use of the high-k gate dielectric technology,[1] the migration from the conventional planar transistor to 3D structures such as the trigate/FinFET,[2,3] or the introduction of embedded stressors in the source and drain to enhance the performance of the device,[4] produced performance benefits of advanced Complementary Metal Oxide Semiconductor (CMOS) technologies. Nevertheless, despite the giant steps taken in recent decades, the continuous pursuit of Moore's law leads us to investigate new solutions to ensure further device shrinkage.[5]

Therefore feasible and interesting alternatives to advanced Silicon (Si) CMOS might lie with transition metal di-chalcogenides, Germanium (Ge), Germanium-Tin (GeSn) alloys, or III-V compounds. Although the integration processing and development costs of these new semiconductor materials are huge, in recent years Ge and its alloy, GeSn, seem to be relatively promising compared to the other candidates; due to their intrinsic characteristics and the relatively easier integration on Si platforms.[6]

Through the years extensive studies on Ge and its alloys have been made in order to explore the possibility to integrate this material in CMOS platforms.[7] Research moved from the physical modelling analysis and characterization[8,9] to process optimization[10,11,12,13] up to the initial planar Field-Effect-Transistor (FET) demonstration. The first outcomes were a starting point which have now progressed onto the development of electrical and optoelectronics devices such as quantum-well devices,[14,15] FinFETs,[16] photodetectors,[17] and lasers[18] that have shown the potential uses of the material.

Nevertheless as FET channel dimensions shrink, the source/drain contact resistance becomes relatively more significant in the overall parasitic resistance in the transistor. In fact

in some cases contact resistance is the bottleneck for certain technologies. Therefore in analogy with Si, where the silicide alloys are used to create metal contacts with low contact resistance, the germanides and stanogermanides, respectively for Ge and GeSn alloys, seem to be natural candidates for metal contacts in these devices. Although Ge solutions proposed have a strong appeal, studies of alloy contacts to GeSn are still immature; consequently an intensive study on contact formation is essential to ensure good GeSn device performance.

Judging from the recent literature on GeSn, much work has been focused on NiGeSn contacts,[19,20,21,22] and on a possible mix among different metals to increase the thermal stability of the alloy.[23,24,25] However, a focused study is still lacking, and is needed, on the contact formation to GeSn using different metals. Therefore, in this work we focused our attention on a systematic and comparative study, using three different metals Ni, Ti, and Pt, on $Ge_{0.92}Sn_{0.08}$. The aim was to determine the best contact alloy candidate in terms of low resistance, low formation temperature, and high thermal stability.

II. EXPERIMENTS

A schematic representation of the process flow and variables considered in this work is shown in Fig. 1. The starting material comprises of a nominally un-doped epi-layer of $Ge_{0.92}Sn_{0.08}$ (28 nm thick) on a nominally un-doped virtual substrate layer of Ge. The Ge layer undergoes 800 °C annealing before growth of $Ge_{0.92}Sn_{0.08}$ to reduce the epi-layer defect density. The un-doped $Ge_{0.92}Sn_{0.08}$ is grown at 320 °C using Ge_2H_6 and $SnCl_4$ in H_2 ambient by chemical vapour deposition

GeSn surfaces were cleaned using a standard recipe; the sample was dipped for 30 s in acetone, 30 s in isopropyl alcohol, and subsequently rinsed under Deionized Water for another 30 s. Thereafter a 10 nm layer of either Ni, Ti or Pt, was deposited on the samples. The metal

deposition was carried out using the FC2000 electron beam evaporator at a pressure of 5×10^{-7} Torr. Ni and Pt were evaporated with a rate of 0.2 nm/s while the Ti with a rate of 0.1 nm/s. Then the samples underwent at 30 s rapid thermal annealing (RTA) in ambient N_2 at different temperatures; ranging from 300 - 500 °C with a difference of 50 °C. The ramp rate used for each RTA was 100 °C/min and the cool down time was 15 min.

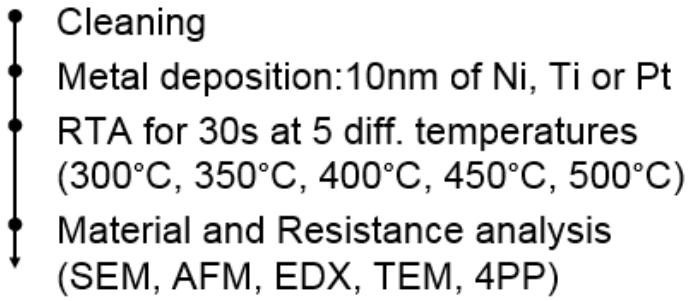

Figure 1: Schematic representation of the stanogermanide process flow and variables considered in this work.

To have a comprehensive study we characterized all the samples as a function of the different RTA temperatures and of the metals used. As regards the material features, the study was performed using Scanning Electron Microscopy (SEM), Atomic Force Microscopy (AFM), cross sectional Transmission Electron Microscopy (TEM) and Electron Dispersive X-ray (EDX); while for the electrical investigation, 4 Point Probe (4PP) analysis was done to extract the sheet resistance of the different stanogermanide materials formed.

SEM surface investigation was performed using a Zeiss Supra55VP machine while the AFM study was carried out with Veeco Multi-mode V AFM in tapping/non-contact mode at room temperature and in air, considering a 5 μm × 5 μm area. Cross-sectioned samples were prepared by focused ion beam etching, using a FEI's Dual Beam Helios Nanolab system using a Ga ion beam. Layers of protective material, consisting of electron beam deposited C, Pt, and ion beam deposited C, were used. Subsequently Cross-sectional Transmission Electron Microscopy (XTEM) was realized using a JEOL 2100 HRTEM operated at 200 kV in bright field mode using a Gatan Double Tilt holder. Scanning TEM imaging as well as point and line-

scan EDX analysis of the cross-sections were performed using FEI's Dual Beam Helios Nanolab system equipped with Oxford Instruments X-MAX-50 EDX detector at 30 kV acceleration voltage. The EDX data collection and quantification was accomplished using software. For the electrical test a 4PP measurement was made using the LUCAS LABS-S-302 4 Manual four point resistivity probing station.

III. RESULTS AND DISCUSSION

A. ELECTRICAL CHARACTERIZATION (4PP)

Fig. 2 shows sheet resistance values measured by the four-point probe measurement.[26]. The plot displays the data obtained for the three different metals as a function of the formation temperature. Ni-Stanogermanide layer shows lower sheet resistance up to a formation temperature of 400 °C, which correlates with that seen for Ge.[27,28] At higher formation temperatures PtGeSn outperforms the NiGeSn in terms of sheet resistance. With regard Ti, the values are approximately one order of magnitude higher compared to the other two materials. Previous research reported in the literature were focused on contact resistance but there are very little data on GeSn sheet resistance.

The resistance results depend on the complete or partial reaction of the metal with the underlying material. This will be discussed further in Sections III.B and III.C. It will be seen that Ni and Pt react readily with the GeSn thin film, while Ti remains unreactive, leading to the poor resistance values seen here. The morphological analysis that follows in Section III.B explores the changing structural trends of the stanogermanides with increased formation temperature. The most interesting condition in Fig. 2, i.e. the lowest measured sheet resistance, NiGeSn formed at 300 °C will be examined in great detail in the lattice imaging study in Section III.C.

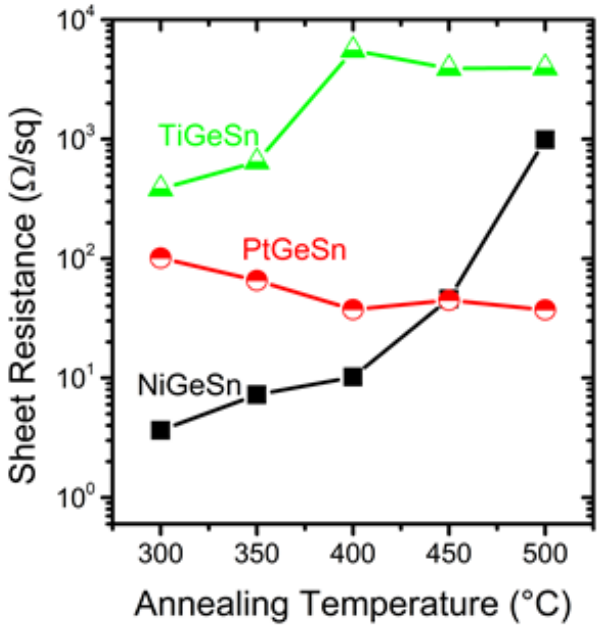

Figure 2: Sheet resistance for Ni, Ti and Pt stanogermanides as a function of the formation temperature.

B. MORPHOLOGICAL ANALYSIS (SEM, AFM, TEM, AND EDX)

All the samples were analysed by SEM to characterize the surface quality as a function of the different metals and formation temperatures used. Fig. 3 shows representative SEM images for the two RTA temperature extremes (300 °C and 500 °C). At 300 °C, all of the Ni, Ti, and Pt samples showed continuous layer formation (Fig. 3(a), 3(c) and 3(e)). In contrast at 500 °C Ni and Ti samples showed the formation of discontinuous layers, while the Pt sample preserved its uniformity, see Fig. 3(b), 3(d) and 3(f). Further SEM analysis revealed that the Ni-stanogermanide reactive growth resulted in continuous layers up to 400 °C, whereby for Ti samples, surface agglomeration started at 450 °C. In comparison, the Pt samples showed continuous structures over the entire temperature range studied. The development of unwanted discontinued layers suggests the formation of island-type inclusions or surface aggregates; further cross-sectional analyses (see below) confirmed that Ni-stanogermanide layers degraded by forming island-type inclusions, while Ti-samples showed surface aggregation at these high temperatures.

In addition, AFM investigations were undertaken on all of the samples; considering a scan area of 5 μm × 5 μm. In all instances, the data was extracted by analysing the central portion of the sample, avoiding edge effects. Fig. 4 highlights the surface roughness of the samples as a function of temperature and metal composition (inset table details the roughness values obtained). For all of the samples analysed, the surface roughness increased with increasing annealing temperature. At 500 °C the NiGeSn and TiGeSn surfaces start to agglomerate, resulting in a root mean square (RMS) roughness around 7 nm. The lowest surface roughness was obtained for PtGeSn. The data obtained are in good accord with previous reports found in literature[29,30] which have shown an increasing roughness with rising annealing temperature for Ni.

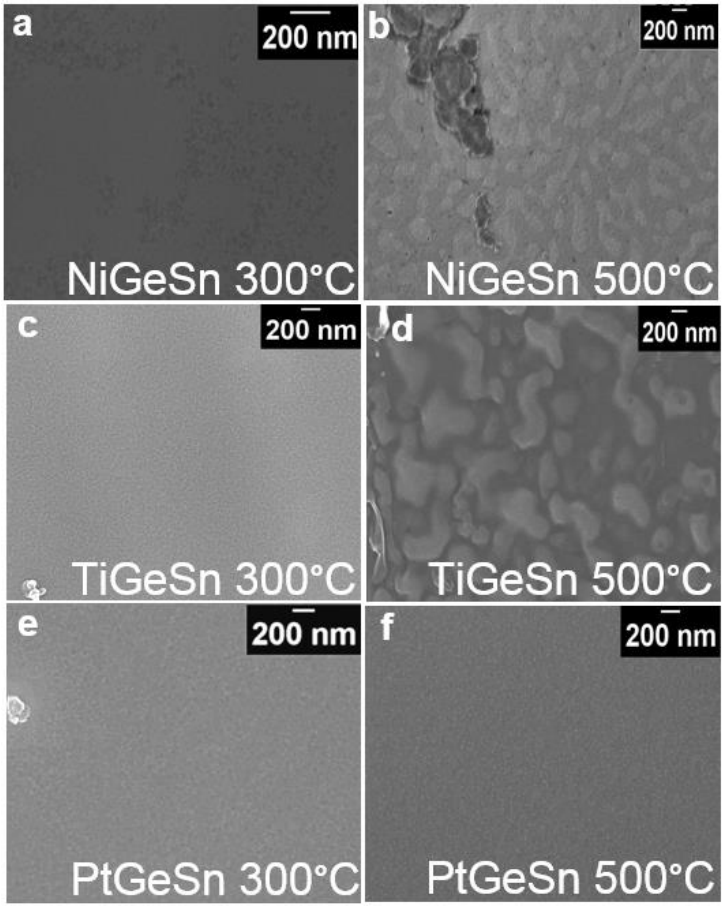

Figure 3: Representative SEM images showing the continuity, or lack of, for the stanogermanides formed in this work; the left-hand column is related to the annealing at 300 °C : a) NiGeSn; c) TiGeSn; e) PtGeSn while the right-hand column refers to the annealing at 500 °C: b) NiGeSn; d) TiGeSn; f) PtGeSn.

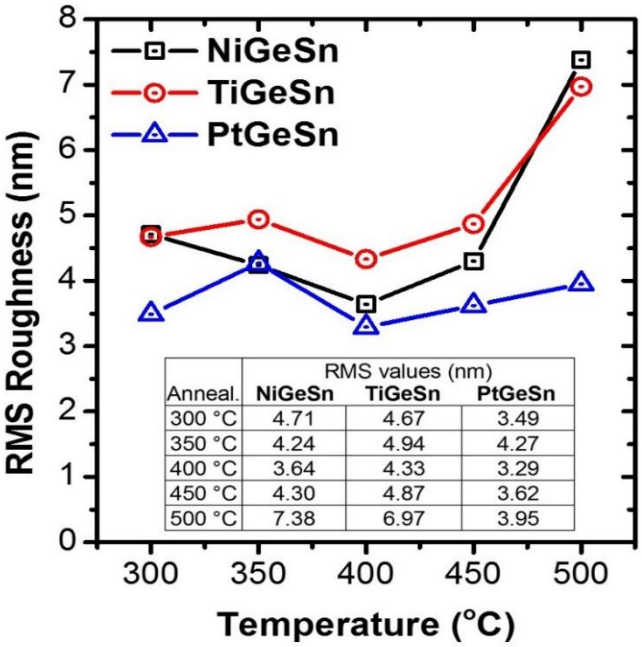

Anneal.	RMS values (nm) NiGeSn	TiGeSn	PtGeSn
300 °C	4.71	4.67	3.49
350 °C	4.24	4.94	4.27
400 °C	3.64	4.33	3.29
450 °C	4.30	4.87	3.62
500 °C	7.38	6.97	3.95

Figure 4: AFM analysis as a function of the different metal and formation temperature. As inset there is a table with all the RMS values of NiGeSn, TiGeSn and PtGeSn formed from 300 °C up to 500 °C.

The thickness and the overall morphology of the metal-GeSn layers after formation at 300 °C and 500 °C were then investigated by cross-sectional TEM analysis (Fig. 5). As shown in Fig. 5(a), 5(c) and 5(e) the cross-sectional analysis confirmed that reactively grown structures, creating surface layer alloys, were formed only with Ni and Pt in this temperature range, while the Ti did not appear to react at 300 °C with the underlying GeSn, displaying a superficial layer of 10 nm. Comparable results have been found as well for the 500 °C RTA process as highlighted in Fig. 5(b), 5(d) and 5(f), in which the Ni and Pt form stanogermanide layers while Ti does not react with the underlying GeSn alloy.

In an overall sense, the solid-state growth process proceeded towards the GeSn layer (nominal thickness of 28 nm) and for the 30 s anneal resulted in structures with different thickness depending on the temperature. The corresponding depth, thickness variation, grain size and stoichiometry (obtained by quantification of point EDX spectra) are summarised in Table 1. Briefly, all Ni and Pt structures were composed of crystal grains with specific size and orientation, justified by observing the variation of the diffraction contrast in the TEM images. In accordance with the top-down SEM analysis (Fig. 3), it was also seen that the continuity of

the NiGeSn layers had degraded at 500 °C, resulting in the formation of well-defined island-type inclusions within the GeSn layer, as shown in Fig. 5(b). In comparison, the PtGeSn structures appeared continuous at both temperatures. Generally, the NiGeSn annealed at 300 °C exhibited the smoothest structure with the largest lateral size of the crystal grains as well as the best quality of the interface with the underlying GeSn. Using EDX analysis on the Ni and Pt samples, we further confirmed that the reactive growth indeed resulted in formation of metal stanogermanides with varying stoichiometry (Table 1).

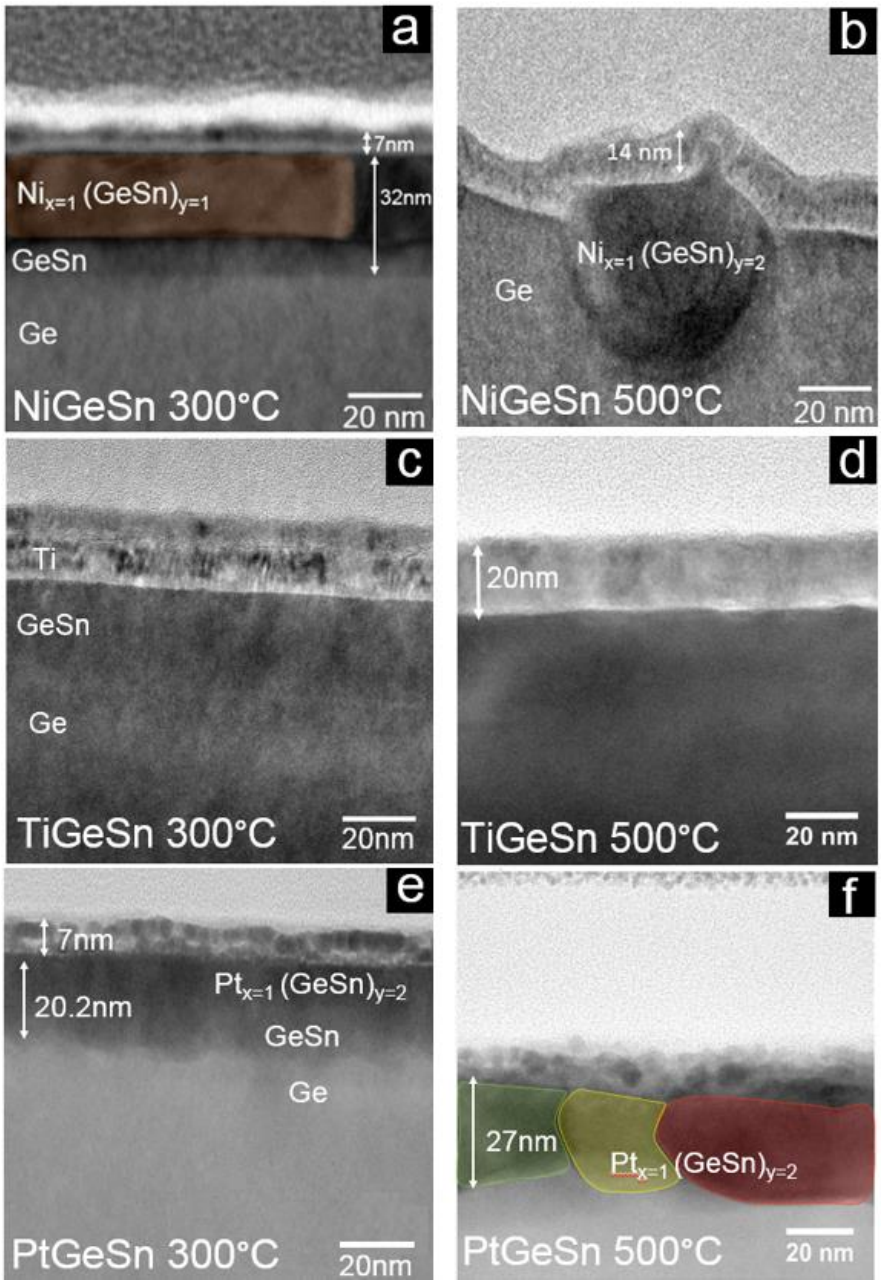

Figure 5 : Representative cross section TEM images at the same magnification with related mixing depth of a) NiGeSn at 300 °C, b) NiGeSn at 500 °C, c) TiGeSn at 300 °C, d) TiGeSn at 500 °C, e) PtGeSn at 300 °C, f) PtGeSn at 500 °C. Colour coded areas depict different grains in the layer.

Sample/Property	Morphology	Thickness (nm)	Lateral grain size (nm)	Composition (line scan EDX) (averaged at.%)
Ni(GeSn) -300 °C	continuous layer	23.5 ±0.6	165 ±9.4	Ge:53; Sn: 4; Ni: 43
-500 °C	inclusions	50.6 ±8.9	132.5 ±34.1	Ge:65; Sn: 1.2; Ni: 33.8
Pt(GeSn) -300 °C	continuous layer	21.3 ±2.6	<10	Ge:59; Sn: 6; Pt: 33
-500 °C	continuous layer	31.3 ±7.4	49.4 ±16.2	Ge:67; Sn: 3.8; Pt: 29.2
Ti(GeSn)	no reaction	-	-	Ge:92; Sn: 8;
Ti(GeSn)	no reaction	-	-	Ge:94; Sn: 6;

Table 1: Summary of the obtained structure for Ni, Pt and Ti annealed at different temperature, from 300 °C up to 500 °C. In the table will be highlighted the morphology the thickness the lateral grain size and the composition of layer formed after the RTA process.

Two major characteristics of the growth process with regards to the composition were observed: i) all samples showed a reduction in the Sn content from the initial non-annealed alloy (nominally the GeSn contained 8 at.% Sn), and ii) formation of Me_x - $(GeSn)_y$ structures with a higher (GeSn) component. The only sample that showed composition that is close to $Me_{x=1}(GeSn)_{y=1}$ is that of the NiGeSn sample formed at 300 °C. Interestingly, the TiGeSn samples (no stanogermanides formed) showed almost no reduction in the Sn content at 300 °C and only a modest reduction at 500 °C in the GeSn layer.

In order to provide further details with regards to the composition of the Ni and Pt structures, EDX line scans were used to obtain compositional profiles for all samples. Figure 6 provides an example of the analysis performed for two samples, Ni and Pt annealed at 300 °C (the rest of the EDX line profile data are presented in the supplementary figures). From the Fig. 6 it can be seen that the Sn content (both averaged values across the stanogermanide layer and point measurements within the layer) decreased to about 4.0 and 6.0 at.% for the Ni and Pt samples, correspondingly. The values decreased further down to 1.2 and 3.8 at.% when the samples were annealed at 500 °C. The Sn content for the non-annealed sample (Fig. 6, blank spec); measured under similar EDX conditions showed a Sn content of about 8.0 at.%; perfectly in accord with the nominal composition for the $Ge_{0.92}Sn_{0.08}$ alloy.

Looking at the Sn EDX profile in the underlying Ge substrate and indeed at the point measurement (Fig. 6, spec 2) at a distance of about 100 nm away from the stanogermanide layer, the Sn signal is within the background noise, which is at the limit-of-the detection of the measurement (about 0.1 at.%). It is worth to mention that the compositional profiles for all Ni_x-$(GeSn)_y$ and Pt_x-$(GeSn)_y$ structures were relatively uniform both across (perpendicular) and along (parallel) the layer surface. Across different grains no major variation in the composition was observed, which can indicate formation of different stanogermanide phases within the layers.

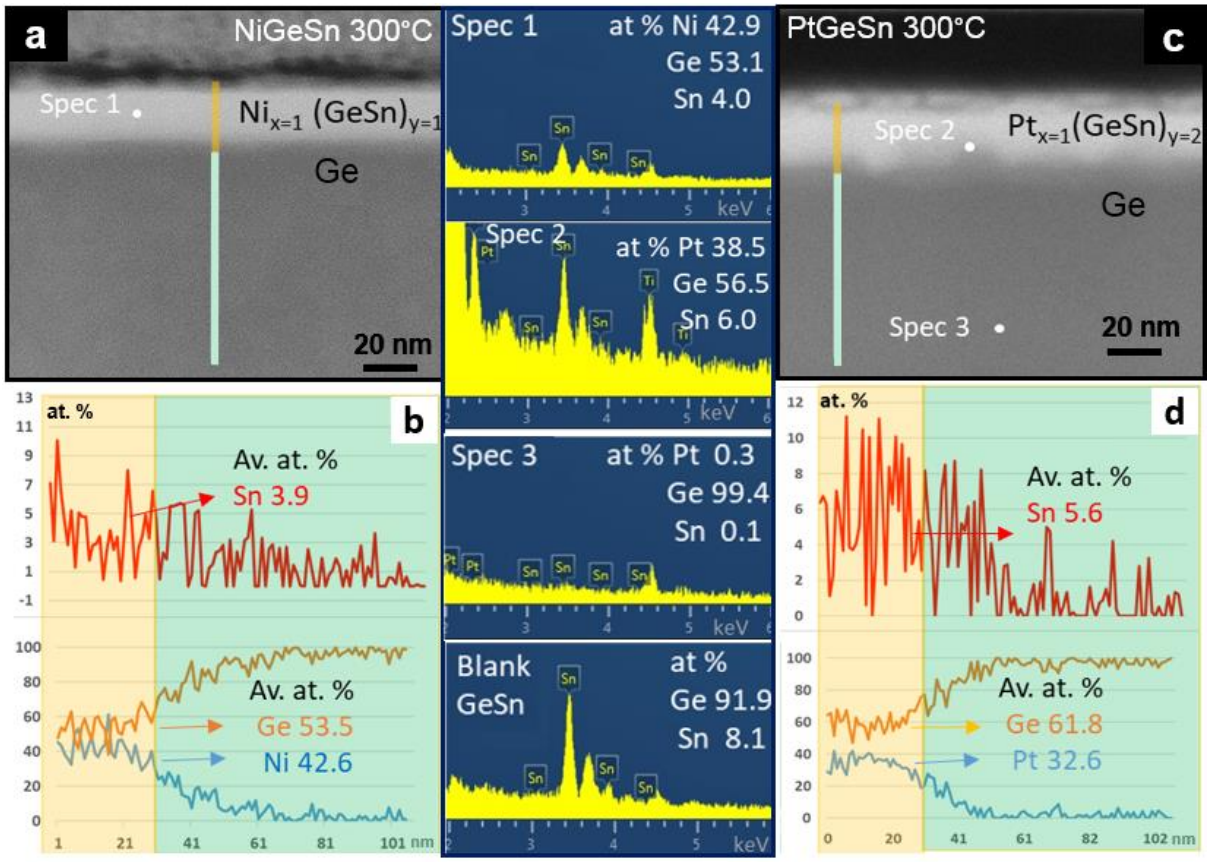

Figure 6: STEM imaging and corresponding EDX line scans for the regions marked with brown and blue measured for the Ni(GeSn) sample (a and b), and Pt(GeSn) sample (c and d), both annealed at 300 °C. Middle column shows EDX point spectra from the marked regions together with the blank GeSn spectrum. Corresponding quant data averaged across the region marked in brown and from the point spectra are also shown.

C. DETAILED LATTICE ANALYSIS

In order to further confirm the corresponding stanogermanide phases formed we performed lattice resolution TEM imaging on several different grains within the layers. Fig. 7(a) shows a lattice resolution TEM image of one of the crystal grains for the NiGeSn sample formed at 300 °C and corresponding Fast Fourier Transformation (FFT) of a selected area from the image. For this grain, the crystal interface with the underlying GeSn appeared abrupt with (111) sets of planes of the $Ni_{x=1}(GeSn)_{y=1}$ phase, at 3.7 degrees misalignment with the (111) set of planes of the GeSn. In comparison, the lattice resolution images for the PtGeSn sample formed at 300 °C showed a variation of crystal orientations of very small (sub-10 nm) crystallites. This is indicated by the FFT pattern shown on Fig. 7(b) whereby all reflections are arranged in diffraction rings.

The most common reflections were with d-spacing of about 3.2 and 2.7 Å that are indicative for existence of (200) and (210) set of planes of the orthorhombic $Pt_{x=1}(GeSn)_{y=2}$ phase. Additional analysis of other crystal grains from the two samples also suggested the appearance of the $Ni_{x=1}(GeSn)_{y=1}$ and $Pt_{x=1}(GeSn)_{y=2}$ phases. In the case of the PtGeSn sample formed at 500 °C, cross-sectional TEM showed the formation of well-developed grains; the lattice resolution image with the corresponding FFT for one such grain is shown on Fig. 7(d).

In the case of a NiGeSn sample annealed at 500 °C, a more distinct change in the morphology compared with a NiGeSn sample formed at 300 °C, *e.g.* formation of island-type inclusions, was observed. The lattice resolution TEM imaging shows in Fig. 7(c) suggested the appearance of $Ni_{x=1}(GeSn)_{y=2}$ phase, evidence by a d-spacing of about 2.7 Å, that corresponds to (400) set of planes of the $Ni_{x=1}(GeSn)_{y=2}$ phase. It is important to note that nickel stanogermanides with higher Ge content are not part of the binary phase diagram. However, we and others have shown that a meta-stable $NiGe_2$ phase exists and it can be produced by using annealing conditions away from equilibrium, as for example laser annealing. Herein we

observed the formation of unusual $Ni_{x=1}(GeSn)_{y=2}$ stanogermanide with relatively low Sn content.

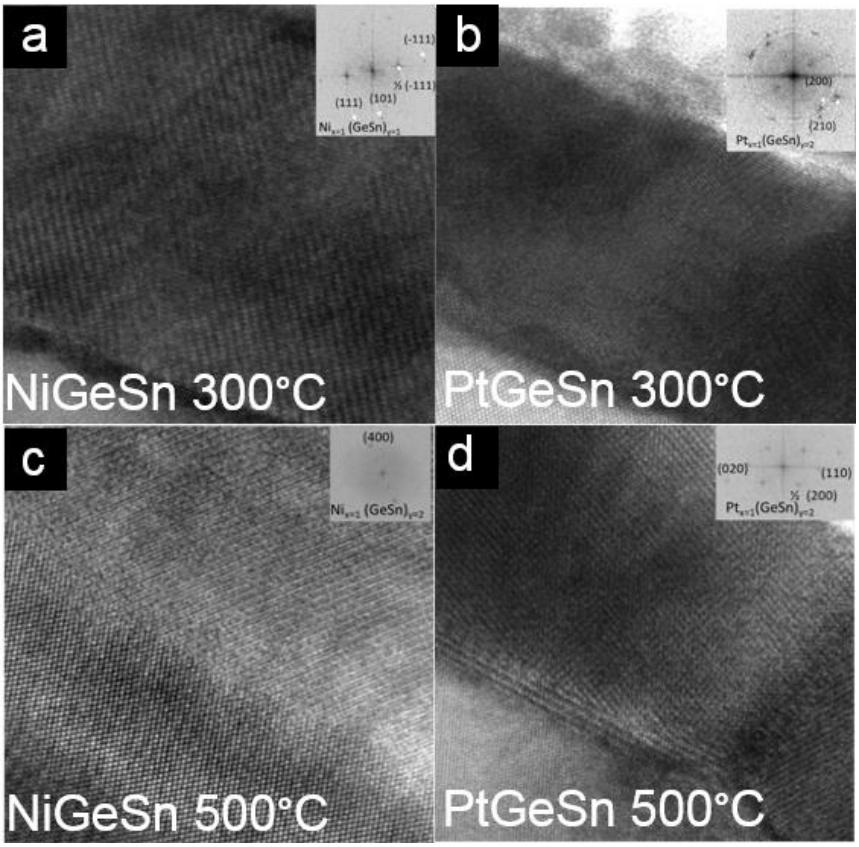

Figure 7: Lattice resolution TEM images of NiGeSn sample formed at 300 °C (a) and 500°C (c), depicting individual crystal grain and of PtGeSn sample formed at 300 °C (b) and 500 °C (d) featuring small crystallites with random orientations. Insets are corresponding FFTs.

Most of the previous research reports focused on the material inspection of the alloy layers and on the contact resistance, even if in few of them, the sheet resistance trend has been stated. Li[19] et al. and Zhang et al.[23] reported an electric and material investigation of NiGeSn under several thermal annealing conditions; in these reports the contact resistivity was found to decrease with increasing annealing temperature, while the defect density increased. Yi Tong at al.[20] studied NiGeSn contact formation, where low resistivity $Ni(Ge_{(1-x)}Sn_{(x)})$ was formed using an annealing temperature of 350°C for 30 seconds. Nishimura et al.[21] showed the formation of NiGeSn layers using a solid phase reaction and investigated the crystalline properties of the layers; the formation of β-Sn was observed after annealing above 450 °C due

to the Sn precipitation and the roughness also degraded as the annealing temperature increased, linked to a poorer thermal stability for samples with high Sn content. Wirths et al.[22] carried out a comprehensive work on the NiGeSn using samples with different Sn percentage. They extracted both morphological and electrical parameters, among which was the sheet resistance as a function of the annealing temperature. Liu et al.[24] and Wang et al.[25] also reported NiGeSn sheet resistance variation. The lowest sheet resistance value was respectively $10\ \Omega/sq$ for Wirths et al. (using an annealing temperature of 325°C) and $5\ \Omega/sq$ for Liu et al. and $6\ \Omega/sq$ Wang et al.; all the benchmarks are comparable with the value that we found in this work ($4\ \Omega/sq$).

IV. CONCLUSIONS

The aim of this research was to show the best metal and formation temperature candidates for stanogermanide contacts on $Ge_{0.92}Sn_{0.08}$ thin films. Ni and Pt are able to form continuous stanogermanide layers over a formation temperature window of 500 °C. NiGeSn showed the best low-resistance performance up to a formation temperature of 400 °C, above which PtGeSn outperformed NiGeSn in terms of sheet resistance. An attractive solution to increase the thermal stability, as long as good electrical and morphological performance are ensured, is represented by a mix of Ni and Pt for stanogermanide formation. For the lowest resistance stanogermanide contact in this work, namely NiGeSn formed at 300 °C, detailed lattice resolution TEM imaging, combined with fast Fourier transformation analysis, identified the formation of the $Ni_{x=1}(GeSn)_{y=1}$ phase.

ACKNOWLEDGEMENTS

We acknowledge the funding support through Science Foundation Ireland Grant Number 14/IA/2513 and MOST 107-2622-8-002-018, and MOST 107-3017-F-009-002. EG acknowledges Dan O'Connell for assistance with sample processing.

REFERENCES

[1] K. Mistry, C. Allen, C. Auth, B. Beattie, D. Bergstrom, M. Bost, M. Brazier, M. Buehler, A. Cappellani, R. Chau*, C.-H. Choi, G. Ding, K. Fischer, T. Ghani, R. Grover, W. Han, D. Hanken, M. Hattendorf, J. He, J. Hicks , R. Huessner, D. Ingerly, P. Jain, R. James, L. Jong, S. Joshi, C. Kenyon, K. Kuhn, K. Lee, H. Liu, J. Maiz, B. McIntyre, P. Moon, J. Neirynck, S. Pae, C. Parker, D. Parsons, C. Prasad, L. Pipes, M. Prince, P. Ranade, T. Reynolds, J. Sandford, L. Shifren°, J. Sebastian, J. Seiple, D. Simon, S. Sivakumar, P. Smith, C. Thomas, T. Troeger, P. Vandervoorn, S. Williams, K. Zawadzki; *Proc. IEEE Int. Electron Devices Meeting* 247, 2007 , 10.1109/IEDM.2007.4418914

[2] C. Auth, C. Allen, A. Blattner, D. Bergstrom, M. Brazier, M. Bost, M. Buehler, V. Chikarmane, T. Ghani, T. Glassman, R. Grover, W. Han, D. Hanken, M. Hattendorf, P. Hentges, R. Heussner, J. Hicks*, D. Ingerly, P. Jain, S. Jaloviar, R. James, D. Jones, J. Jopling, S. Joshi, C. Kenyon, H. Liu, R. McFadden, B. McIntyre, J. Neirynck, C. Parker, L. Pipes, I. Post, S. Pradhan, M. Prince, S. Ramey, T. Reynolds, J. Roesler, J. Sandford, J. Seiple, P. Smith, C. Thomas, D. Towner, T. Troeger, C. Weber, P. Yashar, K. Zawadzki, K. Mistry; Proc. IEEE Symp. On VLSI TEchnol. 131,pp.131-132, 2012, 10.1109/VLSIT.2012.6242496

[3] Klaus Schuegraf, Mathew C. Abraham, Adam Brand, Mehul Naik, and Randhir Thakur, IEEE Journal of the Electron Devices Society, Vol.1, no.3, pp.66-75, 2013 , 10.1109/JEDS.2013.2271582

[4] T. Ghani, M. Armstrong, C. Auth, M. Bost, P. Charvat, G. Glass, T. Hoffiann, K. Johnson, C. Kenyon, J. Klaus, B.Mclntyre, K. Mistry, A. Murthy, 1. Sandford, M. Silberstein, S. Sivakumar, P. Smith, K. Zawadzki, S. Thompson and M. Bohr; Proc. IEEE Int. Electron Devices Meeting, pp.11.6.1-11.6.3, 2003, 10.1109/IEDM.2003.1269442

[5] Dimitri A. Antoniaidis and Ali Khakifirooz; IEEE International Electron Devices Meeting, 2008, 10.1109/IEDM.2008.4796665

[6] S. Gupta, X. Gong, R. Zhang, Y.C. Yeo, S. Takagi and K.C. Saraswat; MRS Bull. 39, pp678-686, 2014, 10.1557/mrs.2014.163

[7] R. Duffy, M. Shayesteh and R.Yu. *Turkish Journal of Physics 38 (2014)* , pp.463-477 10.3906/flz-1405-2

[8] Wang H., Han G., Liu Y., Hu S., Zhang C., Zhang J. and Hao, Y.; "Theoretical Investigation of performance enhancement in GeSn/SiGeSn Type-II staggered heterojunction tunneling FET" (2016) IEEE Transactions on Electron Devices, 63 (1), art. no. 7349191, pp. 303-310. DOI: 10.1109/TED.2015.2503385.

[9] Sant, S. and Schenk, A. "Band-offset engineering for GeSn-SiGeSn hetero tunnel FETs and the role of strain" (2015) IEEE Journal of the Electron Devices Society, 3 (3), art. no. 7006669, pp. 164-175. DOI: 10.1109/JEDS.2015.2390971.

[10] Fang Y.-C., Chen K.-Y., Hsieh C.-H., Su C.-C., Wu Y.-H. "N-MOSFETs formed on solid phase epitaxially grown GeSn film with passivation by oxygen plasma featuring high mobility" (2015) ACS Applied Materials and Interfaces, 7 (48), pp. 26374-26380. DOI: 10.1021/acsami.5b08518.

[11] Schulte-Braucks C. , Glass S. , Hofmann E. , Stange D. , Von Den Driesch N. , Hartmann J., M. Ikonic, Z. Zhao Q. T. , Buca D., Mantl S. ; "Process modules for GeSn nanoelectronics with high Sn-contents" (2017) Solid-State Electronics, 128, pp. 54-59. DOI: 10.1016/j.sse.2016.10.024.

[12] Wirths, S., Troitsch, R., Mussler, G., Zaumseil, P., Hartmann, J.M. Schroeder, T. Mantl, S., Buca, D. Buca; "Ni(SiGeSn) metal contact formation on low bandgap strained (Si)Ge(Sn) Semiconductors" (2014) ECS Transactions, 64 (6), pp. 107-112. DOI: 10.1149/06406.0107ecst.

[13] Prucnal, S., Berencén, Y., Wang, M., Rebohle, L., Böttger, R., Fischer, I.A., Augel, L., Oehme, M., Schulze, J., Voelskow, M., Helm, M., Skorupa, W., Zhou, S. "Ex situ n+ doping of GeSn alloys via non-equilibrium processing" (2018) Semiconductor Science and Technology, 33 (6), art. no. 065008, . DOI: 10.1088/1361-6641/aabe05.

[14] Han, G., Wang, Y., Liu, Y., Zhang, C., Feng, Q., Liu, M., Zhao, S., Cheng, B., Zhang, J., Hao, Y. "GeSn Quantum Well P-Channel Tunneling FETs Fabricated on Si(001) and (111) with Improved Subthreshold Swing" (2016) IEEE Electron Device Letters, 37 (6), art. no. 7460184, pp. 701-704. DOI: 10.1109/LED.2016.2558823.

[15] Huang, Y.-S., Lu, F.-L., Tsou, Y.-J., Ye, H.-Y., Lin, S.-Y., Huang, W.-H., Liu, C.W. "Vertically stacked strained 3-GeSn-Nanosheet pGAAFETs on Si Using GeSn/Ge CVD epitaxial growth and the optimum selective channel release process" (2018) IEEE Electron Device Letters, 39 (9), art. no. 8403243, pp. 1274-1277. DOI: 10.1109/LED.2018.2852775.

[16] Lei, D., Lee, K.H., Bao, S., Wang, W., Masudy-Panah, S., Yadav, S., Kumar, A., Dong, Y., Kang, Y., Xu, S., Wu, Y., Huang, Y.-C., Chung, H., Chu, S.S., Kuppurao, S., Tan, C.S., Gong, X., Yeo, Y.-C. "The first GeSn FinFET on a novel GeSnOI substrate achieving lowest S of 79 mV/decade and record high Gm, int of 807 μs/μm for GeSn P-FETs" (2017) Digest of Technical Papers - Symposium on VLSI Technology, 0, art. no. 7998170, pp. T198-T199. DOI: 10.23919/VLSIT.2017.7998170.

[17] Wang, W., Lei, D., Huang, Y.-C., Lee, K.H., Loke, W.-K., Dong, Y., Xu, S., Tan, C.S., Wang, H., Yoon, S.-F., Gong, X., Yeo, Y.-C. "High-performance GeSn photodetector and fin

field-effect transistor (FinFET) on an advanced GeSn-on-insulator platform" (2018) Optics Express, 26 (8), pp. 10305-10314. DOI: 10.1364/OE.26.010305.

[18] Von Den Driesch, N., Stange, D., Rainko, D., Povstugar, I., Zaumseil, P., Capellini, G., Schröder, T., Denneulin, T., Ikonic, Z., Hartmann, J.-M., Sigg, H., Mantl, S., Grützmacher, D. Buca; "Advanced GeSn/SiGeSn Group IV Heterostructure Lasers" (2018) Advanced Science, 5 (6), art. no. 1700955, . DOI: 10.1002/advs.201700955.

[19] H. Li, H. H. Cheng, L. C. Lee, C. P. Lee, L. H. Su and Y. W. Suen; Applied Physics Letters, 104, 241904, 2014.

[20] Y. Tong, G. Han, B. Liu, Y. Yang, L. Wang, W. Wang and Y. C. Yeo; IEEE Trans. El. Dev. 60, 746, 2013.

[21] T. Nishimura, O. Nakatsuka, Y. Shimura, S. Takeuchi, B. Vincent, A. Vantomme, J. Dekister, M. Caymax, R. Loo and S. Zaima; Solid State Electronics 60, 46, 2011.

[22] S Wirths; R. Troitsch; G. Mussler; J-M Hartmann; P. Zaumseil; T. Schroeder; S. Mantl and D. Buca , Semicond. Sci. Technol. 30, 055003, 2015.

[23] X. Zhang, D. Zhang, J. Zheng, Z. Liu, C. He, C. Xue, G. Zhang, C. Li B. Cheng and Q. Wang; Solid State Electronics 114, 178, 2015.

[24] Y. Liu, H. Wang, J. Yan and G. Han; ECS Solid State Letters 3, 11, 2014.

[25] L. Wang, G. Han, S. Su, Q. Zhou, Y. Yang, P. Guo, W. Wang, Y. Tong. P. S. Y. Lim, E. Y. J. Kong, C. Xue, Q. Wang, B. Cheng and Y. C. Yeo; Electro. Solid State Letters 15, H179, 2012.

[26] F.M Smits The Bell system Technical Journal 37 pp.711-718, 1958, 10.1002/j.1538-7305.1958.tb03883.x

[27] D. P. Brunco, B. De Jaeger, G. Eneman, J. Mitard, G. Hellings, A. Satta,V. Terzieva, L. Souriau, F. E. Leys, G. Pourtois, M. Houssa, G. Winderickx, E. Vrancken, S. Sioncke, K. Opsomer, G. Nicholas, M. Caymax, A. Stesmans,b J. Van Steenbergen, P. W. Mertens, M.

Meuris, and M. M. Heyns; Journal of the Electochemical society, vol.155 (7), pp. H552-H561, 2008, 10.1149/1.2919115

[28] S.Gaudet, C. Detavernier, A.J. Kellock, P. Desjardins, C. Lavoie ;*J. Vac. Sci. technol. A*, Vol. 24, No.3, pp. 474-485 , 2006, 10.1116/1.2191861

[29] Tsuyoshi Nishimura, Osamu Nakatsuka, Yosuke Shimura, Shotaro Takeuchi, Benjamin Vincent, Andre Vantomme, Johan Dekoster, Matty Caymax, Roger Loo, Shigeaki Zaima, Solid State Electronics, Vol. 60 , pp. 46-52, 2011, 10.1016/j.sse.2011.01.025

[30] W. Wan, W. Ren, X. Meng. Y. Ping, X. Wei, Z. Xue, W. Yu, M. Zhang, Z. Di, B. Zhang, Chin.Phys.Lett., Vol. 35, No. 5, 056802, 2018 10.1088/0256-307X/35/5/056802